

# A NUMERICAL COMPARISON BETWEEN DEGENERATE PARABOLIC AND QUASILINEAR HYPERBOLIC MODELS OF CELL MOVEMENTS UNDER CHEMOTAXIS

M. TWAROGOWSKA<sup>1</sup>, R. NATALINI<sup>1</sup>, AND M. RIBOT<sup>2</sup>

ABSTRACT. We consider two models which were both designed to describe the movement of eukaryotic cells responding to chemical signals. Besides a common standard parabolic equation for the diffusion of a chemoattractant, like chemokines or growth factors, the two models differ for the equations describing the movement of cells. The first model is based on a quasilinear hyperbolic system with damping, the other one on a degenerate parabolic equation. The two models have the same stationary solutions, which may contain some regions with vacuum. We first explain in details how to discretize the quasilinear hyperbolic system through an upwinding technique, which uses an adapted reconstruction, which is able to deal with the transitions to vacuum. Then we concentrate on the analysis of asymptotic preserving properties of the scheme towards a discretization of the parabolic equation, obtained in the large time and large damping limit, in order to present a numerical comparison between the asymptotic behavior of these two models. Finally we perform an accurate numerical comparison of the two models in the time asymptotic regime, which shows that the respective solutions have a quite different behavior for large times.

## 1. INTRODUCTION

The movement of cells, bacteria or other microorganisms under the effect of a chemical stimulus, represented by a chemoattractant, such as chemokines or growth factors, has been widely studied in mathematics in the last two decades, see [25, 30, 31, 38], and various models involving partial differential equations have been proposed to describe this evolution. The basic unknowns in these chemotactic models are the density of individuals and the concentrations of some chemical attractants. One of the most considered models is the Patlak-Keller-Segel system [27, 36], where the evolution of the density of cells is described by a parabolic equation, and the concentration of a chemoattractant is generally given by a parabolic or elliptic equation, depending on the different regimes to be described and on

---

*keywords and phrases:* chemotaxis, quasilinear hyperbolic problems with source, degenerate parabolic problems, comparison between parabolic and hyperbolic models, stationary solutions with vacuum, well-balanced scheme, asymptotic behavior.

<sup>1</sup> Istituto per le Applicazioni del Calcolo “Mauro Picone”, Consiglio Nazionale delle Ricerche, via dei Taurini 19, I-00185 Roma, Italy (mtwarogowska@gmail.com, roberto.natalini@cnr.it).

<sup>2</sup> Laboratoire J. A. Dieudonné, UMR CNRS 7351, Université de Nice-Sophia Antipolis, Parc Valrose, F-06108 Nice Cedex 02, France & Project Team COFFEE, INRIA Sophia Antipolis, France (ribot@unice.fr).

the authors' taste. The behavior of this systems is quite well known now, at least for linear diffusions: in the one-dimensional case, the solution is always global in time [32], while in two and more dimensions the solutions exist globally in time or blow up according to the size of the initial data, see [9, 10] and references therein, and see the recent result of global existence for large data in the parabolic-parabolic case [4]. However, a drawback of this model is that the diffusion leads alternatively to a fast dissipation or an explosive behavior, while in general, from a biological point of view, it is much more interesting to observe the creation of patterns and permanent structures.

In order to avoid these drawbacks and to improve the accuracy of the transient description, some modifications of the original Keller-Segel formulation were introduced to prevent overcrowding, by taking into account the volume filling effect; see [25, 38, 23, 35]. For instance, in [28, 8], a nonlinear diffusion is considered. More precisely, denoting by  $\rho(x,t)$  the density of cells and by  $\phi(x,t)$  the concentration of a generic chemoattractant, the Keller-Segel-like system with nonlinear diffusion reads

$$\begin{cases} \rho_t = P(\rho)_{xx} - \chi(\rho\phi_x)_x, \\ \delta\phi_t = D\phi_{xx} + a\rho - b\phi, \end{cases} \quad (1)$$

where  $\chi, D, a$  and  $b$  are given positive parameters. The cells move following the direction of the gradient of the concentration of chemoattractant with a response coefficient  $\chi$ ; they also diffuse and  $P$  is a phenomenological, density dependent function, which is usually given by a pressure law for isentropic gases, such as

$$P(\rho) = \kappa\rho^\gamma, \quad \gamma > 1, \quad \kappa > 0, \quad (2)$$

which is intended to prevent the overcrowding of cells. Besides, the evolution of chemoattractant is still given by a linear diffusion equation with a source term which depends on  $\rho$ . The chemoattractant is released by the cells, diffuses in the environment and it is degraded in finite time. The positive parameters  $D, a, b$  are respectively its diffusion coefficient, the production rate, which is proportional to the cell density, and the degradation rate. If  $\delta = 1$ , we consider a parabolic-parabolic model and in the case where  $\delta = 0$ , we deal with a parabolic-elliptic model.

Now, it is also expected that a hyperbolic model will enable us to observe intermediate organized structures, like aggregation patterns, at a finer scale [37]. In [14, 24] the advantage of the hyperbolic approach over the parabolic one was considered in the case of a semilinear model of chemotaxis based on the Cattaneo law. In particular, the authors described qualitatively some experiments of patterns formation. Here, we focus on a quasilinear hyperbolic model of chemotaxis introduced by Gamba et al. [17] to describe the early stages of the vasculogenesis process. This model writes as a hyperbolic-parabolic system for the following unknowns: the density of cells  $\rho(x,t)$ , their momentum  $\rho u(x,t)$  and the concentration  $\phi(x,t)$  of a chemoattractant:

$$\begin{cases} \rho_t + (\rho u)_x = 0, \\ (\rho u)_t + (\rho u^2 + P(\rho))_x = -\alpha\rho u + \chi\rho\phi_x, \\ \phi_t = D\phi_{xx} + a\rho - b\phi. \end{cases} \quad (3)$$

The positive constants  $\chi$  and  $\alpha$  measure respectively the strength of the cells response to the concentration of the chemical substance and the strength of the damping forces. The pressure  $P$  is still given by the pressure law for isentropic gases (2). This model of chemotaxis has been introduced to describe the results of in vitro experiments performed by Serini et al. [41] using human endothelial cells which, randomly seeded on a matrigel, formed complex patterns with structures depending on the initial number of cells.

Although analytical results about this model are still far from being complete, for the Cauchy problem on the whole space and in all space dimensions, so with no boundary conditions, it is possible to prove the global existence of smooth solutions if the initial datum is a small perturbation of a small enough constant state, see [12, 13]. In the case of the one dimensional boundary value problem, when the differential part is linearized, the global existence and the time asymptotic decay of the solutions were proved in [22], if the initial data are small perturbations of stable constant stationary states. To complete the analytical study of the quasilinear model there are some clear difficulties. The first one lies in the appearance of regions of vacuum during the evolution of the time solution, since the hyperbolic part of the model degenerates as the eigenvalues coincide; as far as we know, the only related results are given in [26, 21], and they are about the local existence of solutions for the Euler equations with damping and vacuum, but without chemotaxis.

From a more biological point of view, the appearance of non constant solutions with a succession of regions with high density of cells and regions of vacuum, can be put in correspondence with the formation of patterns, such as a network of blood capillaries. In [34], present authors analyzed the existence of some non-constant steady states to model (3) on a one dimensional bounded domain. In particular, for the pressure law (2) with  $\gamma=2$ , a complete description of the stationary solutions formed of one region of positive density near the boundary and one region of vacuum was given. Numerical simulations also shown that such solutions are stable and can be found as asymptotic states of the system (3) even for strictly positive initial data. In the following, we will call "bump" a region with a nonnegative density surrounded by two regions of vacuum, as shown in blue in Figure 1, and a "lateral half bump" will be a bump cut in its middle and stuck to an extremity of the interval, as shown in red in the same Figure 1. Other stationary configurations with several bumps have been also observed numerically as asymptotic states of the model in [34]. These configurations are described in details with a comparison of their energy values in [3].

Remark that in the case of bounded domains with no-flux boundary conditions, stationary solutions for both systems (3) and (1) coincide and it is worth exploring if the asymptotic states of the two systems are the same or not. Actually, one may expect the Keller-Segel type model (1) with  $\delta=0$  (i.e.: the parabolic-elliptic case) to be the large time and large damping limit of the hyperbolic system (3), and this is actually the case in [29] for the case without chemotaxis or in [11] for our case, both results being proved only on unbounded domains. In this paper, our main goal is to make a careful comparison of the two models (3) and (1) with  $\delta=1$ ,

by analyzing numerically their actual asymptotic behavior. In particular, we are able to exhibit some sets of initial data and some parameters such that the two systems converge asymptotically to two different stationary solutions, namely two solutions with a different number of bumps. In that case, the diffusive Keller-Segel model (1) seems to be more inclined to merge bumps together, so that the asymptotic solution contains a smaller number of bumps than the asymptotic solution for the hyperbolic system (3), often after a long transient where nothing happens. Some similar phenomena which are referred as metastability of patterns, were observed in the case of a Keller-Segel type model with linear diffusion and a logistic chemosensitive function in [23, 40, 15], see Subsection 5.3 for more details.

In order to perform such a comparison, we need first to find an accurate scheme for the hyperbolic system to make a reliable comparison of the two models. The approximation of this system needs special care due to the presence of vacuum states and emergence of non-constant steady states. More precisely, the discretization procedure has to generate non-negative solutions with finite speed of propagation and should resolve properly the non constant equilibria, characterized by a vanishing flux. Such problems are well-known when dealing with hyperbolic equations with sources, see for instance [33, 18, 20, 19]. For that purpose, we consider the well-balanced scheme proposed in [34] and based on the Upwinding Sources at Interfaces methodology [5, 6, 39]. In [34], we used a hydrostatic reconstruction, introduced by Audusse et al. [2] in the case of shallow-water equations and by Bouchut, Ounaissa and Perthame [7] in the case of Euler equations with large damping. To use this approach, we compute the reconstructed interface variables by integrating the equation for stationary solutions with a constant velocity. According to the form of the equation we integrate, two different reconstructions can be found; both lead to schemes that are consistent with the hyperbolic problem, preserve the non-negativity of the density, and are exact on non-constant steady states. However, we show in this paper that only one of these two schemes is asymptotically consistent with a conservative scheme for the parabolic model in the large time and large damping limit, and therefore it will be the one used in our comparison. Another improvement of the scheme described here, with respect with [34], is the implicit treatment of the damping term, which solves more accurately the vacuum states and the flux on the non constant equilibria.

This paper is organized as follows: after a brief recall in Section 2 about the structure of the stationary solutions with vacuum, found in [34] and [3], we propose in Section 3 two different numerical schemes for the quasilinear hyperbolic system (3) based on well-balanced techniques, with a particular care for their asymptotic preserving property. Then, in Section 4, we show some numerical evidences of the behavior of these schemes in order to choose a well adapted scheme. Finally, in Section 5, we present an accurate scheme for the parabolic system (1), based on the diffusive relaxation techniques of [1], and we perform a careful numerical comparison between the asymptotic solutions for systems (3) and for system (1).

## 2. STATIONARY SOLUTIONS WITH VACUUM

In [34] and [3], we noticed that in the particular case  $\gamma=2$ , it is possible to compute explicitly and classify the stationary solutions with vacuum of the two systems (3) and (1), which obviously coincide. Let us recall briefly these results to make the paper almost self-contained.

Consider system (3) on a one dimensional bounded domain  $[0, L]$  with no-flux boundary conditions, that is

$$\rho_x(0, \cdot) = \rho_x(L, \cdot) = 0, \quad \rho u(0, \cdot) = \rho u(L, \cdot) = 0, \quad \phi_x(0, \cdot) = \phi_x(L, \cdot) = 0. \quad (4)$$

Notice that, under these conditions, the stationary solutions of system (3) and system (1) coincide. Remark also that, when considering the evolution problem (3) or (1) with the previous boundary conditions (4), the mass of the density is constant in time, namely

$$M = \int_{[0, L]} \rho(x, 0) dx = \int_{[0, L]} \rho(x, t) dx, \quad \text{for all } t \geq 0. \quad (5)$$

Therefore, the mass  $M$  will be considered in what follows as a parameter which characterizes stationary solutions.

**2.1. Constant solution.** The first type of solutions is given by the constant solutions, that is to say, for all domain length  $L > 0$  and all mass  $M > 0$ , there is a solution defined by  $(\rho, u, \phi) = (\frac{M}{L}, 0, \frac{aM}{bL})$ , which is the only constant solution in the space of stationary states. This kind of solution is displayed in green in Figure 1.

**2.2. One lateral half bump.** Let us denote by  $\omega = \frac{1}{D} \left( \frac{a\chi}{2\kappa} - b \right)$ . We assume that  $\omega > 0$  and  $L > \frac{\pi}{\sqrt{\omega}}$ . Then there exists a unique, positive solution (up to symmetry) of mass  $M$  with only one region of positive density and one region of vacuum, given by the following expression :

$$\rho(x) = \begin{cases} \frac{\chi}{2\kappa} \phi(x) + K, & \text{for } x \in [0, \bar{x}], \\ 0, & \text{for } x \in (\bar{x}, L], \end{cases} \quad (6a)$$

and

$$\phi(x) = \begin{cases} \frac{2\kappa b K \cos(\sqrt{\omega} x)}{\omega \chi D \cos(\sqrt{\omega} \bar{x})} - \frac{aK}{\omega D}, & \text{for } x \in [0, \bar{x}], \\ -\frac{2\kappa K \cosh(\sqrt{\frac{b}{D}}(x-L))}{\chi \cosh(\sqrt{\frac{b}{D}}(\bar{x}-L))}, & \text{for } x \in (\bar{x}, L]. \end{cases} \quad (6b)$$

The free boundary point  $\bar{x}$  is given by the only value  $\bar{x} \in \frac{1}{\sqrt{\omega}}(\pi/2, \pi)$  which solves the equation

$$\sqrt{\frac{b}{\omega D}} \tan(\sqrt{\omega} \bar{x}) = \tanh\left(\sqrt{\frac{b}{D}}(\bar{x}-L)\right), \quad (6c)$$

and the constant  $K$  is equal to

$$K = \frac{D}{b} \frac{M\omega^{3/2}}{\tan(\sqrt{\omega}\bar{x}) - \sqrt{\omega}\bar{x}}. \quad (6d)$$

If  $\omega < 0$ , or  $\omega > 0$ , but  $L < \frac{\pi}{\sqrt{\omega}}$ , then there is no half bump solution to the problem.

An example of such solution is plotted in red in Figure 1.

**2.3. Other configurations.** In [34], we also proved that, in the case when  $L > \frac{2\pi}{\sqrt{\omega}}$ , there exists only one solution composed by a central bump surrounded by two regions of vacuum. This solution is symmetric with respect to the middle point of the interval  $[0, L]$  and can be computed by sticking two lateral bumps, calculated on a domain  $[0, L/2]$  with a mass  $M/2$ . This can be seen in blue in Figure 1.

In [3], it is shown that, when a two bumps solution, which is made by a concatenation of two bumps (in the case  $L > \frac{4\pi}{\sqrt{\omega}}$ ), is computed, then one can find an infinite number of such solutions. Namely, there is one parameter free in the family of such solutions. Moreover, for each solution, an energy can be calculated and it can be proved that the symmetric two bumps solution has the higher energy (in cyan in Figure 1), whereas the solution with no vacuum for one of the two bumps has the lower one (in black in Figure 1). It is also possible to construct some 3-bumps solutions with 2 parameters, and so on. We expect all these stationary solutions to exist for any other values of  $\gamma > 1$ , but for  $\gamma \neq 2$ , it is difficult to work, since we have no more explicit expressions of the solutions. To conclude this section, let us say that, among all these configurations, the constant solution has the highest energy, whereas the lateral half bump is the one with lowest energy, see again [3].

In Figure 1, we can see five different types of stationary solutions for the same parameters of the system, always with  $\gamma = 2$ , same length of the domain  $L$  and same mass  $M$ . The densities are obtained analytically using the above formulas, while the locations of interfaces with vacuum  $\bar{x}$  are found by solving equation (6c) numerically.

### 3. A NUMERICAL APPROXIMATION FOR THE QUASILINEAR HYPERBOLIC MODEL

Let us now explain how to construct a well adapted scheme for system (3), taking care of being accurate in the approximation of stationary solutions. System (3) couples equations of different natures, i.e. a quasilinear system of conservation laws with sources, which is coupled with a linear parabolic equation. The latter is very classical and several methods can be used, as, for instance, finite differences in space and the classical explicit-implicit Crank-Nicholson method for the time discretization. Now, in this section, we concentrate on the discretization of the hyperbolic part and we improve the finite volume scheme proposed in [34], based on the Upwinding Sources at the Interfaces technique developed in [6, 5, 2, 7].

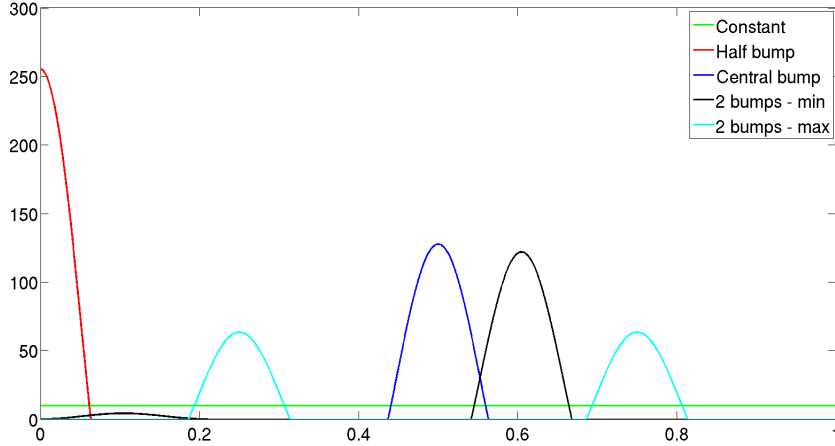


FIGURE 1. Various stationary solutions: constant (in green), one lateral half bump (in red), one central bump (in blue), two bumps with minimal energy (in black), two symmetric bumps with maximal energy (in cyan). The parameters are the following :  $\kappa = 1$ ,  $\chi = 10$ ,  $D = 0.1$ ,  $a = 20$ ,  $b = 10$ ,  $L = 1$  and  $M = 10$ .

After a brief recall about the numerical framework, we analyze the asymptotic preserving property in the large time and large damping limit, which is given by the parabolic system (1) with  $\delta = 0$ . We show that E-reconstruction (12) is not asymptotic preserving, whereas the P-reconstruction (13) is consistent, in the large time and large damping limit, with a conservative scheme for the parabolic problem.

**3.1. Finite volume, well-balanced scheme.** Denoting by  $U = (\rho, \rho u)^T$  the vector of two unknowns, respectively density and momentum, the hyperbolic part of system (3) can be written in the following form

$$U_t + F(U)_x = S(U), \quad (7a)$$

where  $F$  is the flux function and  $S$  the source term, i.e.

$$F(U) = \begin{pmatrix} F^\rho \\ F^{\rho u} \end{pmatrix} = \begin{pmatrix} \rho u \\ \rho u^2 + P(\rho) \end{pmatrix}, \quad S(U) = \begin{pmatrix} 0 \\ -\alpha \rho u + \chi \rho \phi_x \end{pmatrix}. \quad (7b)$$

According to the framework of finite volume schemes, we divide the interval  $[0, L]$  into  $N$  cells  $C_i = [x_{i-1/2}, x_{i+1/2})$ , centered at the nodes  $x_i$ ,  $1 \leq i \leq N$ . In the following, we assume that all the cells have the same length  $\Delta x = x_{i+1/2} - x_{i-1/2}$ . We consider a semi-discrete space approximation of the solution  $U$  to system (7) on cell  $C_i$ , i.e. we compute an approximation of the cell average of the solution at time  $t > 0$ , that is to say

$$U_i(t) = \frac{1}{\Delta x} \int_{x_{i-1/2}}^{x_{i+1/2}} U(x, t) dx.$$

We denote now by  $U_i^n$  an approximation of function  $U_i(t)$  at discrete time  $t_n = n\Delta t$ , where  $\Delta t$  is the time step. Let us consider a numerical flux

$\mathcal{F} = \begin{pmatrix} \mathcal{F}^\rho \\ \mathcal{F}^{\rho u} \end{pmatrix}$  consistent with the continuous flux  $F$ , that is to say that it satisfies

$$\mathcal{F}(U, U) = F(U) \text{ for all } U. \quad (8)$$

A general, fully discrete, explicit finite volume scheme for (7) can be written as

$$\frac{\Delta x}{\Delta t} (U_i^{n+1} - U_i^n) + \mathcal{F}(U_{i+1/2}^{n,-}, U_{i+1/2}^{n,+}) - \mathcal{F}(U_{i-1/2}^{n,-}, U_{i-1/2}^{n,+}) = \mathcal{S}_i^n, \quad (9a)$$

where the values  $U_{i+1/2}^{n,\pm}$  are interface variables computed at the point  $x_{i+1/2}$ , and  $\mathcal{S}_i^n$  is an approximation of the source term.

According to the results in [34], we decided to discretize the homogeneous part using the Suliciu scheme adapted to vacuum, see also [6]. Notice that in the following, we may write  $\mathcal{F}(\rho_{i+1/2}^{n,-}, u_{i+1/2}^{n,-}, \rho_{i+1/2}^{n,+}, u_{i+1/2}^{n,+})$  instead of  $\mathcal{F}(U_{i+1/2}^{n,-}, U_{i+1/2}^{n,+})$  when necessary.

### 3.2. Upwinding Sources at the Interfaces and reconstructions.

Following [34], we compute the interfaces variables in order to preserve non-constant stationary solutions with constant velocity. We also need to upwind the source term and we use the following ansatz :

$$\mathcal{S}_i^n = \mathcal{S}_{i+1/2}^{n,-} + \mathcal{S}_{i-1/2}^{n,+} = \begin{pmatrix} 0 \\ P(\rho_{i+1/2}^{n,-}) - P(\rho_i^n) + P(\rho_i^n) - P(\rho_{i-1/2}^{n,+}) \end{pmatrix}. \quad (9b)$$

This ansatz is based on the equation satisfied by stationary solutions i.e.  $F(U)_x = S(U)$  and the fact that the momentum of a stationary solution is vanishing, thanks to the boundary conditions (4).

We also reconstruct the interface variables  $U_{i+1/2}^{n,\pm}$  using the local equilibrium

$$u_x = 0, \quad (P(\rho))_x = \chi \rho \phi_x - \alpha \rho u. \quad (10)$$

To derive our first method, we observe that the second equation can be rewritten in terms of the internal energy  $e(\rho)$  defined by  $e'(\rho) = \frac{P(\rho)}{\rho^2}$ , which yields

$$(\Psi(\rho) - \chi \phi)_x = -\alpha u, \text{ with } \Psi(\rho) = e(\rho) + \frac{P(\rho)}{\rho} = \frac{\kappa \gamma}{\gamma - 1} \rho^{\gamma-1}. \quad (11)$$

From this equation, we obtain the so-called E-reconstruction, by an approximate integration on  $[x_i, x_{i+1/2}^-)$  and  $(x_{i+1/2}^+, x_{i+1}]$ , by taking:

$$u_{i+1/2}^{n,-} = u_i^n, \quad u_{i+1/2}^{n,+} = u_{i+1}^n \quad (12a)$$

and

$$\begin{cases} \Psi(\rho_{i+1/2}^{n,-}) = [\Psi(\rho_i^n) + \chi(\min(\phi_i^n, \phi_{i+1}^n) - \phi_i^n) - \alpha(u_i^n)_+ \Delta x]_+, \\ \Psi(\rho_{i+1/2}^{n,+}) = [\Psi(\rho_{i+1}^n) + \chi(\min(\phi_i^n, \phi_{i+1}^n) - \phi_{i+1}^n) + \alpha(u_{i+1}^n)_- \Delta x]_+. \end{cases} \quad (12b)$$

We proved in [34] that the scheme (9), coupled with the E- reconstruction (12), is consistent with system (3) away from vacuum, preserves the



non-negativity of the density and preserves the stationary solutions with vanishing velocity.

Another way to proceed is to integrate directly the equilibrium equation (10) to get a different reconstruction, namely:

$$u_{i+1/2}^{n,-} = u_i^n, \quad u_{i+1/2}^{n,+} = u_{i+1}^n \quad (13a)$$

and

$$\begin{cases} P(\rho_{i+1/2}^{n,-}) = \left[ P(\rho_i^n) + \chi \bar{\rho}_{i+1/2}^n (\min(\phi_i^n, \phi_{i+1}^n) - \phi_i^n) - \alpha \rho_i^n (u_i^n)_+ \Delta x \right]_+, \\ P(\rho_{i+1/2}^{n,+}) = \left[ P(\rho_{i+1}^n) + \chi \bar{\rho}_{i+1/2}^n (\min(\phi_i^n, \phi_{i+1}^n) - \phi_{i+1}^n) \right. \\ \qquad \qquad \qquad \qquad \qquad \qquad \qquad \qquad \qquad \qquad \qquad \qquad \qquad \left. + \alpha \rho_{i+1}^n (u_{i+1}^n)_- \Delta x \right]_+, \end{cases} \quad (13b)$$

where  $\bar{\rho}_{i+1/2}^n = \frac{1}{2}(\rho_i^n + \rho_{i+1}^n)$ . In the following this scheme will be mentioned as the P-reconstruction.

The computations to prove that the scheme (9), coupled with the P-reconstruction (13) is consistent, preserves the non-negativity of the density and preserves the stationary solutions with vanishing velocity, are analogous to the ones performed in [34] for the E-reconstruction. Moreover, as shown in [34], this scheme is stable under a condition of the form

$$\sigma(U_{i+1/2}^{n,-}, U_{i+1/2}^{n,+}) \Delta t \leq \Delta x,$$

where  $\sigma(U_i, U_{i+1})$  is a numerical speed such that the solver  $\mathcal{F} = (\mathcal{F}^\rho, \mathcal{F}^{\rho u})^t$  for the homogeneous system  $U_t + F(U)_x = 0$  preserves the non negativity of  $\rho$  by interface; see [34] or [6] for more details.

Next, we propose another possible improvement for our scheme, which consists in discretizing implicitly the damping term. Indeed, in the previous reconstructions (12) and (13), the damping term was included in the definition of the interface densities. However, since it is a stiff term, it is more natural to deal with an implicit treatment. Therefore, the damping term is considered in the discretization equation and disappears in the reconstruction formula; the second equation of the fully discrete scheme (9) is therefore replaced by :

$$\begin{aligned} (\rho u)_i^{n+1} &= (\rho u)_i^n - \frac{\Delta t}{\Delta x} \left( \mathcal{F}^{\rho u}(\hat{U}_{i+1/2}^{n,-}, \hat{U}_{i+1/2}^{n,+}) - \mathcal{F}^{\rho u}(\hat{U}_{i-1/2}^{n,-}, \hat{U}_{i-1/2}^{n,+}) \right) \\ &\quad + \frac{\Delta t}{\Delta x} \left( P(\hat{\rho}_{i+1/2}^{n,-}) - P(\hat{\rho}_{i-1/2}^{n,+}) \right) - \alpha \Delta t (\rho u)_i^{n+1}, \end{aligned} \quad (14a)$$

with

$$\hat{u}_{i+1/2}^{n,-} = u_i^n, \quad \hat{u}_{i+1/2}^{n,+} = u_{i+1}^n \quad (14b)$$

and the interface values are given respectively by

$$\begin{cases} \Psi(\hat{\rho}_{i+1/2}^{n,-}) = \left[ \Psi(\rho_i^n) + \chi (\min(\phi_i^n, \phi_{i+1}^n) - \phi_i^n) \right]_+, \\ \Psi(\hat{\rho}_{i+1/2}^{n,+}) = \left[ \Psi(\rho_{i+1}^n) + \chi (\min(\phi_i^n, \phi_{i+1}^n) - \phi_{i+1}^n) \right]_+, \end{cases} \quad (14c)$$

for the E-reconstruction, and by

$$\begin{cases} P\left(\hat{\rho}_{i+1/2}^{n,-}\right) = \left[ P(\rho_i^n) + \chi \bar{\rho}_{i+1/2}^n (\min(\phi_i^n, \phi_{i+1}^n) - \phi_i^n) \right]_+, \\ P\left(\hat{\rho}_{i+1/2}^{n,+}\right) = \left[ P(\rho_{i+1}^n) + \chi \bar{\rho}_{i+1/2}^n (\min(\phi_i^n, \phi_{i+1}^n) - \phi_{i+1}^n) \right]_+, \end{cases} \quad (14d)$$

for the P-reconstruction. Next, let us study the convergence of these various schemes in the large time and large damping limit.

**3.3. The asymptotic preserving property.** We are now going to show that, using a large time and large damping scaling (LTLTD in the following) in system (3), we obtain a chemotaxis model based on the porous medium equation. Recall that, in [29], it was proven that the velocity of the compressible Euler system without chemotaxis satisfies the Darcy law in the large time limit, while in [11] the asymptotic convergence of system (3) to parabolic systems was analyzed under various scalings. Both papers were dealing with the case of the whole space.

Here, on the contrary, we are in a bounded interval, and so space dilations are not considered. Therefore, let  $\varepsilon = \frac{1}{\alpha} > 0$  and define the following scaled variables, to perform the LTLTD limit:

$$\tau = \varepsilon t, \quad v^\varepsilon(x, \tau) = \frac{u(x, t)}{\varepsilon}, \quad \rho^\varepsilon(x, \tau) = \rho(x, t), \quad \phi^\varepsilon(x, \tau) = \phi(x, t).$$

Hence, system (3) can be rewritten for the new unknowns as :

$$\begin{cases} \rho_\tau^\varepsilon + (\rho^\varepsilon v^\varepsilon)_x = 0 \\ \varepsilon^2 (\rho^\varepsilon v^\varepsilon)_\tau + [\varepsilon^2 \rho^\varepsilon (v^\varepsilon)^2 + P(\rho^\varepsilon)]_x = \chi \rho^\varepsilon \phi_x^\varepsilon - \rho^\varepsilon v^\varepsilon \\ \varepsilon \phi_\tau^\varepsilon = D \phi_{xx}^\varepsilon + a \rho^\varepsilon - b \phi^\varepsilon \end{cases} \quad (15)$$

As  $\varepsilon \rightarrow 0$ , which corresponds to the LTLTD limit, we obtain the following parabolic-elliptic system, see [11] for more analytical details, that is system (1) with  $\delta = 0$  :

$$\begin{cases} \rho_\tau = [P(\rho)_{xx} - \chi(\rho \phi_x)_x] \\ 0 = D \phi_{xx} + a \rho - b \phi. \end{cases} \quad (16)$$

In this section, we study the asymptotic preserving property of the numerical scheme (9) with the reconstruction (12) or (13) for system (3). Following [7], we compute the LTLTD limit of the first component of the numerical flux  $\mathcal{F}^\rho$  obtained with the two methods of reconstruction for system (15) and we analyze their consistency with system (16). More precisely, we say that a numerical flux is asymptotic preserving in the LTLTD limit, if we have the following local expansion:

$$\mathcal{F}^\rho \left( \rho_{i+1/2}^{\varepsilon, n, -}, u_i^n, \rho_{i+1/2}^{\varepsilon, n, +}, u_{i+1}^n \right) = \mathcal{F}_{i+1/2}^{n, \text{Par}} + O(\varepsilon \Delta x) + O(\varepsilon^2),$$

where  $\mathcal{F}_{i+1/2}^{n, \text{Par}}$  is a consistent and conservative numerical flux for the parabolic equation :

$$\rho_t = (P(\rho)_x - \chi(\rho \phi_x))_x.$$

We show in the following theorem that this property depends on the reconstruction we choose.

To handle correctly the proof of the theorem, we need the following conditions on the numerical flux :

**Definition 3.1.** A consistent numerical flux function  $\mathcal{F}$  is said to be strongly consistent if it satisfies the two following conditions :

- if  $\mathcal{F}^{\rho u}(r, 0, R, 0) = P(r)$  then  $r = R$ ;
- if  $\mathcal{F}^{\rho u}(r, 0, R, 0) = P(R)$  then  $r = R$ .

This definition is derived from a condition given in [7] and is satisfied, in particular, for the HLL flux, the HLL-Roe flux and the Suliciu relaxation flux adapted to vacuum (see [6]). In the annex 6, the reader can find a discussion about this condition and the computations to prove that the previous fluxes satisfy it.

**Theorem 3.2.** Assume that the hyperbolic numerical flux  $\mathcal{F}$  is consistent with the continuous flux  $F$  defined in equation (7b) and strongly consistent in the sense of Definition 3.1. Assume also the following asymptotic expansions for  $\rho_i^n$  and  $u_i^n$  when  $\varepsilon \rightarrow 0$ :

$$\rho_i^{\varepsilon, n} = r_i^n + \varepsilon r_i^{n, (1)} + O(\varepsilon^2), \quad u_i^{\varepsilon, n} = \varepsilon v_i^{\varepsilon, n} = \varepsilon v_i^{n, (0)} + \varepsilon^2 v_i^{n, (1)} + O(\varepsilon^3). \quad (17)$$

Then, we have that

$$\begin{aligned} \mathcal{F}^\rho \left( \rho_{i+1/2}^{\varepsilon, -}, u_i, \rho_{i+1/2}^{\varepsilon, +}, u_{i+1} \right) &= -\frac{1}{\Delta x} \left( P(r_{i+1}) - P(r_i) + \chi \bar{r}_{i+1/2} (\phi_i - \phi_{i+1}) \right) \\ &\quad + O(\varepsilon \Delta x) + O(\varepsilon^2) \end{aligned}$$

in the case of the P-reconstruction and

$$\begin{aligned} \mathcal{F}^\rho \left( \rho_{i+1/2}^{\varepsilon, -}, u_i, \rho_{i+1/2}^{\varepsilon, +}, u_{i+1} \right) &= -\frac{r_i}{\Delta x} \left( \Psi(r_{i+1}) - \Psi(r_i) + \chi (\phi_i - \phi_{i+1}) \right) \\ &\quad + O(\varepsilon \Delta x) + O(\varepsilon^2). \end{aligned}$$

in the case of the E-reconstruction.

Therefore, in the case of the isentropic gases pressure (2), only the P-reconstruction is asymptotic preserving in the LTLTD limit.

*Proof.* We first pass to the limit  $\varepsilon \rightarrow 0$  in the second equation of scheme (9), using expansions (17), and we obtain that

$$\mathcal{F}^{\rho u} \left( r_{i+1/2}^{n, -}, 0, r_{i+1/2}^{n, +}, 0 \right) - \mathcal{F}^{\rho u} \left( r_{i-1/2}^{n, -}, 0, r_{i-1/2}^{n, +}, 0 \right) = P \left( r_{i+1/2}^{n, -} \right) - P \left( r_{i-1/2}^{n, +} \right).$$

Thanks to the assumption of strong consistency of the flux, the relation  $r_{i+1/2}^{n, -} = r_{i+1/2}^{n, +}$  gives a unique solution to the previous equation; see annex 6 for more details.

We now pass into the limit  $\varepsilon \rightarrow 0$  in the first equation of scheme (9). The asymptotic expansion of  $\mathcal{F}^\rho \left( \rho_{i+1/2}^{\varepsilon, n, -}, u_i^n, \rho_{i+1/2}^{\varepsilon, n, +}, u_{i+1}^n \right)$  around a state  $\left( \rho_{i+1/2}^{\varepsilon, n, -}, u_i^n, \rho_{i+1/2}^{\varepsilon, n, -}, u_i^n \right)$  is, dropping the  $n$  index when there is no confusion:

$$\begin{aligned} \mathcal{F}^\rho \left( \rho_{i+1/2}^{\varepsilon, -}, u_i, \rho_{i+1/2}^{\varepsilon, +}, u_{i+1} \right) &= \mathcal{F}^\rho \left( \rho_{i+1/2}^{\varepsilon, -}, u_i, \rho_{i+1/2}^{\varepsilon, -}, u_i \right) \\ &\quad + \left( \rho_{i+1/2}^{\varepsilon, +} - \rho_{i+1/2}^{\varepsilon, -} \right) (\partial_3 \mathcal{F}^\rho) + (u_{i+1} - u_i) (\partial_4 \mathcal{F}^\rho) + O \left( \rho_{i+1/2}^{\varepsilon, +} - \rho_{i+1/2}^{\varepsilon, -} \right)^2 \\ &\quad + O \left( u_{i+1} - u_i \right)^2, \end{aligned} \quad (18)$$

where  $\partial_i \mathcal{F}^\rho$  is the derivative of  $\mathcal{F}^\rho$  with respect to the  $i$ -th variable calculated at point  $\left( \rho_{i+1/2}^{\varepsilon, n, -}, u_i^n, \rho_{i+1/2}^{\varepsilon, n, -}, u_i^n \right)$ .

Let us now estimate all these terms separately. It is first easy to see that  $(u_{i+1} - u_i) = \varepsilon \Delta x$ , from expansions (17). Now, using the consistency of  $\mathcal{F}^\rho$ , we have :

$$\mathcal{F}^\rho \left( \rho_{i+1/2}^{\varepsilon,-}, u_i, \rho_{i+1/2}^{\varepsilon,-}, u_i \right) = F^\rho(\rho_{i+1/2}^{\varepsilon,-}, u_i) = \rho_{i+1/2}^{\varepsilon,-} u_i = (\rho_{i+1/2}^{\varepsilon,-} - \rho_i^\varepsilon) u_i + \rho_i^\varepsilon u_i.$$

Using the P-reconstruction (13) or the E-reconstruction (12) for  $\rho_{i+1/2}^{\varepsilon,\pm}$  and the asymptotic expansion (17), we have  $(\rho_{i+1/2}^{\varepsilon,-} - \rho_i^\varepsilon) u_i = O(\varepsilon \Delta x)$ .

*Case of the P-reconstruction.* Let us now estimate the two remaining terms  $\rho_i^\varepsilon u_i$  and  $\rho_{i+1/2}^{\varepsilon,+} - \rho_{i+1/2}^{\varepsilon,-}$  in the case of the P-reconstruction. Passing to the limit in the reconstruction (13) when  $\varepsilon \rightarrow 0$ , we obtain

$$\begin{cases} P \left( r_{i+1/2}^- \right) = [P(r_i) + \chi \bar{r}_{i+1/2} (\min(\phi_i, \phi_{i+1}) - \phi_i) - r_i (u_i)_+ \Delta x]_+, \\ P \left( r_{i+1/2}^+ \right) = [P(r_{i+1}) + \chi \bar{r}_{i+1/2} (\min(\phi_i, \phi_{i+1}) - \phi_{i+1}) + r_{i+1} (u_{i+1})_- \Delta x]_+ \end{cases}$$

and using that  $r_{i+1/2}^{n,-} = r_{i+1/2}^{n,+}$ , we obtain by subtracting the two previous equations and dropping the positive part:

$$0 = P(r_{i+1}) - P(r_i) + \chi \bar{r}_{i+1/2} (\phi_i - \phi_{i+1}) + (r_{i+1} (u_{i+1})_- + r_i (u_i)_+) \Delta x. \quad (19)$$

By the same way, subtracting the two equations (13) and dropping the positive part, we also obtain the following equation :

$$\begin{aligned} P \left( \rho_{i+1/2}^{\varepsilon,+} \right) - P \left( \rho_{i+1/2}^{\varepsilon,-} \right) &= P(\rho_{i+1}^\varepsilon) - P(\rho_i^\varepsilon) + \chi \bar{\rho}_{i+1/2}^\varepsilon (\phi_i - \phi_{i+1}) \\ &+ (\rho_{i+1}^\varepsilon (u_{i+1})_- + \rho_i^\varepsilon (u_i)_+) \Delta x. \end{aligned} \quad (20)$$

Now, subtracting (20) and (19) gives :

$$\begin{aligned} P \left( \rho_{i+1/2}^{\varepsilon,+} \right) - P \left( \rho_{i+1/2}^{\varepsilon,-} \right) &= (P(\rho_{i+1}^\varepsilon) - P(\rho_i^\varepsilon)) - (P(r_{i+1}) - P(r_i)) \\ &+ ((\rho_{i+1}^\varepsilon - r_{i+1})(u_{i+1})_- + (\rho_i^\varepsilon - r_i)(u_i)_+) \Delta x \\ &+ \chi (\bar{\rho}_{i+1/2}^\varepsilon - \bar{r}_{i+1/2}) (\phi_i - \phi_{i+1}). \end{aligned}$$

Under this previous form and using the expansions (17), it is straightforward that  $P \left( \rho_{i+1/2}^{\varepsilon,+} \right) - P \left( \rho_{i+1/2}^{\varepsilon,-} \right) = O(\varepsilon \Delta x) + O(\varepsilon^2)$  and, consequently, that  $\rho_{i+1/2}^{\varepsilon,+} - \rho_{i+1/2}^{\varepsilon,-} = O(\varepsilon \Delta x) + O(\varepsilon^2)$ .

Finally, let us consider the last term  $\rho_i^\varepsilon u_i$  of (18). Using expansions (17), we decompose it as follows, in order to use relation (19) :

$$\begin{aligned} \rho_i^\varepsilon u_i &= \rho_i^\varepsilon ((u_i)_+ + (u_i)_-) = \rho_i^\varepsilon (u_i)_+ + \rho_{i+1}^\varepsilon (u_{i+1})_- + O(\varepsilon \Delta x), \\ &= r_i (u_i)_+ + r_{i+1} (u_{i+1})_- + O(\varepsilon^2) + O(\varepsilon \Delta x) \end{aligned}$$

which gives

$$\rho_i^\varepsilon u_i = -\frac{1}{\Delta x} (P(r_{i+1}) - P(r_i) + \chi \bar{r}_{i+1/2} (\phi_i - \phi_{i+1})) + O(\varepsilon^2) + O(\varepsilon \Delta x).$$

To conclude, all these estimates enable us to write equation (18) in the case of the P-reconstruction as :

$$\begin{aligned} \mathcal{F}^\rho \left( \rho_{i+1/2}^{\varepsilon,-}, u_i, \rho_{i+1/2}^{\varepsilon,+}, u_{i+1} \right) &= -\frac{1}{\Delta x} (P(r_{i+1}) - P(r_i) + \chi \bar{r}_{i+1/2} (\phi_i - \phi_{i+1})) \\ &+ O(\varepsilon \Delta x) + O(\varepsilon^2). \end{aligned}$$

*Case of the E-reconstruction.* We follow the same computations as for the P-reconstruction. We estimate the two remaining terms  $\rho_i^\varepsilon u_i$  and  $\rho_{i+1/2}^{\varepsilon,+} - \rho_{i+1/2}^{\varepsilon,-}$  in the case of the E-reconstruction. Passing to the limit in the reconstruction (12) when  $\varepsilon \rightarrow 0$ , we obtain

$$\begin{cases} \Psi\left(r_{i+1/2}^-\right) = [\Psi(r_i^n) + \chi(\min(\phi_i^n, \phi_{i+1}^n) - \phi_i^n) - (u_i^n)_+ \Delta x]_+, \\ \Psi\left(r_{i+1/2}^+\right) = [\Psi(r_{i+1}^n) + \chi(\min(\phi_i^n, \phi_{i+1}^n) - \phi_{i+1}^n) + (u_{i+1}^n)_- \Delta x]_+. \end{cases}$$

and using that  $r_{i+1/2}^{n,-} = r_{i+1/2}^{n,+}$ , we obtain by subtracting the two previous equations and dropping the positive part:

$$0 = \Psi(r_{i+1}) - \Psi(r_i) + \chi(\phi_i - \phi_{i+1}) + ((u_{i+1})_- + (u_i)_+) \Delta x. \quad (21)$$

By the same way, subtracting the two equations (12) and dropping the positive part, we also obtain the following equation :

$$\begin{aligned} \Psi\left(\rho_{i+1/2}^{\varepsilon,+}\right) - \Psi\left(\rho_{i+1/2}^{\varepsilon,-}\right) &= \Psi(\rho_{i+1}^\varepsilon) - \Psi(\rho_i^\varepsilon) + \chi(\phi_i - \phi_{i+1}) \\ &+ ((u_{i+1})_- + (u_i)_+) \Delta x. \end{aligned} \quad (22)$$

Now, subtracting (22) and (21) gives :

$$\Psi\left(\rho_{i+1/2}^{\varepsilon,+}\right) - \Psi\left(\rho_{i+1/2}^{\varepsilon,-}\right) = (\Psi(\rho_{i+1}^\varepsilon) - \Psi(\rho_i^\varepsilon)) - (\Psi(r_{i+1}) - \Psi(r_i)).$$

Using the expansions (17), it is straightforward that  $\rho_{i+1/2}^{\varepsilon,+} - \rho_{i+1/2}^{\varepsilon,-} = O(\varepsilon \Delta x) + O(\varepsilon^2)$ .

Finally, let us consider the last term  $\rho_i^\varepsilon u_i$  of (18). Using expansions (17), we decompose it as follows, in order to use relation (21) :

$$\begin{aligned} \rho_i^\varepsilon u_i &= \rho_i^\varepsilon ((u_i)_+ + (u_i)_-) = \rho_i^\varepsilon ((u_i)_+ + (u_{i+1})_-) + O(\varepsilon \Delta x), \\ &= r_i ((u_i)_+ + (u_{i+1})_-) + O(\varepsilon^2) + O(\varepsilon \Delta x) \end{aligned}$$

which gives

$$\rho_i^\varepsilon u_i = -\frac{r_i}{\Delta x} (\Psi(r_{i+1}) - \Psi(r_i) + \chi(\phi_i - \phi_{i+1})) + O(\varepsilon^2) + O(\varepsilon \Delta x).$$

To conclude, all these estimates enable us to write equation (18) in the case of the E-reconstruction as :

$$\begin{aligned} \mathcal{F}^\rho\left(\rho_{i+1/2}^{\varepsilon,-}, u_i, \rho_{i+1/2}^{\varepsilon,+}, u_{i+1}\right) &= -\frac{r_i}{\Delta x} (\Psi(r_{i+1}) - \Psi(r_i) + \chi(\phi_i - \phi_{i+1})) \\ &+ O(\varepsilon \Delta x) + O(\varepsilon^2). \end{aligned}$$

□

Following (11), we can see that the second result of the theorem can be rewritten as :

$$\begin{aligned} \mathcal{F}^\rho\left(\rho_{i+1/2}^{\varepsilon,-}, u_i, \rho_{i+1/2}^{\varepsilon,+}, u_{i+1}\right) &= -\frac{r_i}{\Delta x} \left( \frac{\kappa\gamma}{\gamma-1} (r_{i+1}^{\gamma-1} - r_i^{\gamma-1}) + \chi(\phi_i - \phi_{i+1}) \right) \\ &+ O(\varepsilon \Delta x) + O(\varepsilon^2). \end{aligned}$$

in the case of the E-reconstruction and of the pressure law for isentropic gases (2). This means that, using the E-reconstruction (12), we obtain in the LTLTD limit, a numerical scheme for the parabolic-elliptic equation (16) which is non-conservative and which has a wrong diffusion coefficient. On

the other hand, the P-reconstruction (13) used in the numerical scheme (9) is consistent with the second order conservative scheme for the Keller-Segel type model (16). In the following, we would therefore rather use the P-reconstruction in our numerical tests.

#### 4. NUMERICAL TESTS FOR THE HYPERBOLIC MODEL

In this section we compare numerically the methods presented in the previous section. We show that the implicit treatment of the damping term gives a better approximation of the momentum and of the density near the vacuum states. Then, choosing the P-reconstruction and the implicit treatment of the damping, we analyze the dependence of the asymptotic numerical solutions on the mesh refinement .

Let us observe that, in the following, we will display several plots of the residuals of the density with respect to time in a log-log scale. The residuals at discrete time  $t^n = n\Delta t$  are defined by the difference of the density between time  $t^{n+1}$  and time  $t^n$ , that is to say  $\|\rho^{n+1} - \rho^n\|$ , and the evolution of the residuals stops whenever we reach a stationary asymptotic solution.

To begin with, let us compare implicit and explicit treatment of the damping term in the momentum balance equation. In what follows, we will use the Suliciu relaxation scheme adapted to vacuum for the homogeneous part of the hyperbolic system for  $\rho$  in (3) and the parabolic equation for  $\phi$  of system (3) is treated thanks to a classical centered discretization in space and a Crank-Nicolson scheme in time.

**4.1. Implicit vs. explicit approximations of the damping term.** In section 3.2, we proposed a partially implicit version of the well-balanced scheme, see equation (14), by treating in a different way the linear stiff damping term of the momentum equation of system (3). Indeed in the well-balanced scheme presented in [34], we treated this term explicitly inside the new reconstructed variables. In this test, we study the effect of this implicit treatment.

We consider system (3) on an interval of length  $L=1$  with the following parameters :  $\gamma=2$  or  $\gamma=3$ ,  $\chi=50$ ,  $D=a=b=\alpha=\kappa=1$ . We take as initial datum the density defined as  $\rho_0(x) = 1 + \sin(4\pi|x - 0.25L|)$ . Figure 2 (respectively Figure 3) displays the solution to system (3) for  $\gamma=2$  (resp.  $\gamma=3$ ) at time  $T=300$  obtained with the various well-balanced schemes presented in section 3.2. More precisely, the figures on the top show the density  $\rho$  and the concentration  $\phi$ , whereas the subfigures on the bottom show the logarithm of the momentum,  $\log|\rho u|$  as a function of the space variable  $x$ . On the left, the P-reconstruction (13) or (14d) is used, whereas on the right, the reconstruction is given by the E-reconstruction (12) or (14c). Finally, on each subfigure, the implicit treatment of the damping term, given by scheme (14) is compared with its explicit integration, that is to say using the schemes (9)-(13)-(12) .

We notice that the two reconstruction methods give comparable results; however, there is a large improvement when the damping term is treated implicitly. It is especially visible for the momentum function, which should vanish asymptotically. In particular, it gives better accuracy in the region where the density vanishes. For the explicit approximation, in the case  $\gamma=3$ ,

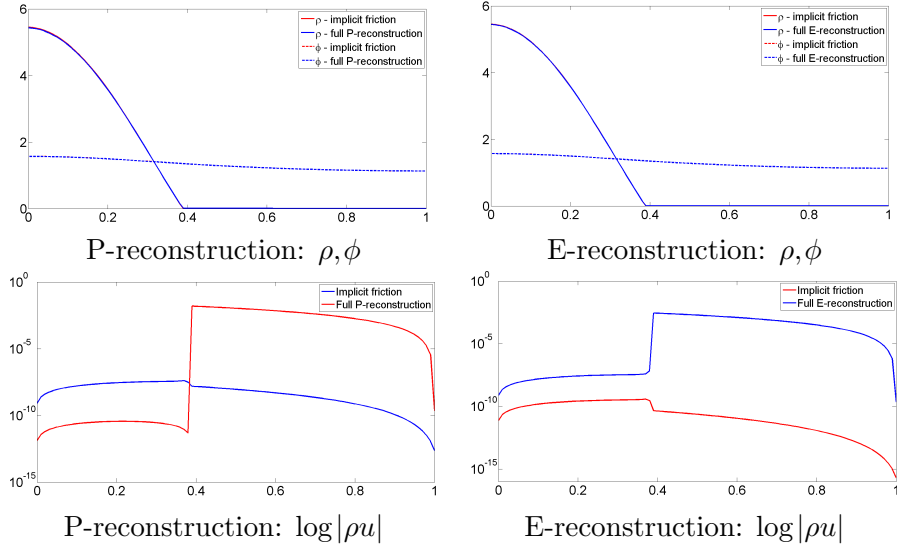


FIGURE 2. Case of the lateral bump with  $\gamma=2$ : Density and concentration distributions (on top) and the logarithm of the momentum (on bottom) for the model (3) with  $\chi=50$ ,  $D=a=b=\alpha=\kappa=1$  and  $\gamma=2$ . Comparison between the P-reconstruction (on the left) and the E-reconstruction (on the right). On each subfigure, the implicit treatment of the damping term is compared with the explicit approximation.

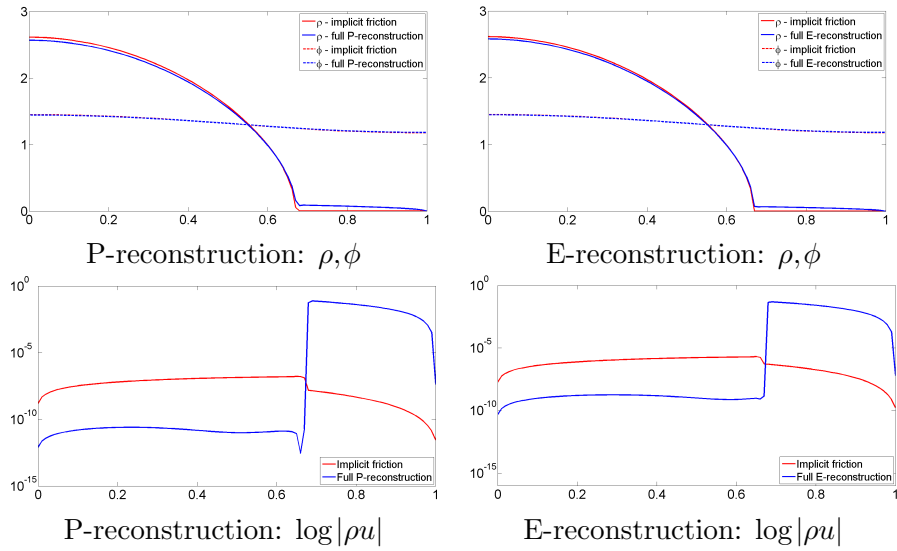


FIGURE 3. Case of the lateral bump with  $\gamma=3$ : Density and concentration distributions (on top) and the logarithm of the momentum (on bottom) for the model (3) with  $\chi=50$ ,  $D=a=b=\alpha=\kappa=1$  and  $\gamma=3$ . Comparison between the P-reconstruction (on the left) and the E-reconstruction (on the right). On each subfigures, the implicit treatment of the damping term is compared with the explicit approximation.

the density and the momentum are far from being zero at the theoretical vacuum states. We remark that in this case, the implicit approximation reduces the  $L^\infty$  error of the momentum of an order  $10^6 - 10^8$ .

In subsection 3.3, we have shown that only the P-reconstruction is asymptotically consistent with a numerical scheme for the correct limit parabolic model. This is the reason why, from now on, we will use the finite volume scheme (9) with the P-reconstruction (14d) and the implicit treatment of the damping term.

**4.2. Mesh dependence.** In computational fluid dynamics (CFD) it is well known that characteristic phenomena of the flow appear at different length scales, and so we have to study the influence of grid refinement on the numerical approximation of solutions. Unlike standard fluid dynamics problems, for which the areas where small scale phenomena may occur are known and static, or their evolution is known, so that adaptive mesh refinement can be applied, for model (3) of chemotaxis, the situation is more complicated since we do not have any information on the precise location of the critical regions, especially vacuum regions. In order to compare correctly the asymptotic behavior of the hyperbolic and parabolic models of chemotaxis in section 5, we analyze first the effect of the mesh refinement on the solutions to the hyperbolic model using the iterative refining process. At first step, we run the simulation on a coarse mesh up to the convergence, that is until a steady solution with vanishing velocity is reached. Then, we refine the mesh uniformly and run the simulation again. If the successive result bears sufficient similarities, the iterative refinement is stopped and the first mesh can be considered as an accurate one. Otherwise, we repeat the mesh refinement until the benefit gained by using the finest mesh is no more significant.

As mentioned before, we use the implicit scheme (14) with the P-reconstruction (14d). It is difficult to choose a good mesh-dependence test that would reflect all the possible behaviors of the model. This is why we analyze the case which will be used as a comparison between the parabolic and the hyperbolic models. We consider system (3) on an interval of length  $L=3$  with the following parameters  $\gamma=2$  or  $\gamma=3$ ,  $\chi=10$ ,  $D=0.1$ ,  $a=20$ ,  $b=10$ ,  $\alpha=\kappa=1$ . We take as an initial datum, the density  $\rho_0(x)=1.5+\sin(4\pi|x-0.25L|)$  and the initial concentration  $\phi=0$ . Figure 4 (resp. 5) shows, on the left, the density as a function of space, using different space steps in the case  $\gamma=2$  (resp.  $\gamma=3$ ). On the right, we display the evolution of the residuals of the density with respect to time using a log-log scale.

We observe that for  $\gamma=2$ , the asymptotic solutions change significantly with the mesh refinement. More precisely, when we decrease the space step  $\Delta x$ , some of the neighboring bumps merge together and the total number of regions with positive density becomes smaller. Finally the only correct solution appears to be the one for  $\Delta x=5 \times 10^{-3}$ , which is stable under further refinements of the mesh. In the case  $\gamma=3$ , the dependence on the mesh size is weaker and the difference is visible only for a very coarse mesh  $\Delta x=5 \times 10^{-2}$ . Below  $\Delta x=2.5 \times 10^{-2}$ , the asymptotic state does not change with the mesh refinement. Moreover, we see that the structure of the



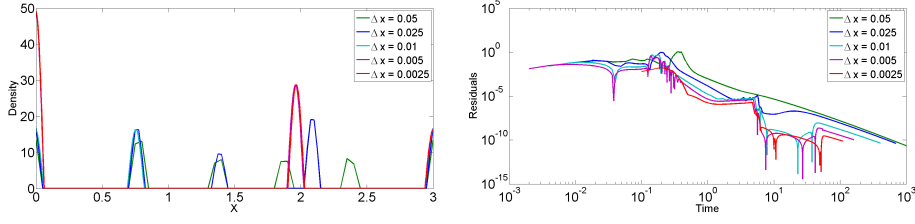


FIGURE 4. Mesh refinement in the case  $\gamma=2$ . Density distribution as a function of space (on the left) and residuals of the density as a function of time in a log-log scale (on the right) for the model (3) with  $\chi=10$ ,  $D=0.1$ ,  $a=20$ ,  $b=10$ ,  $\alpha=\kappa=1$  and  $\gamma=2$ , approximated using the P-reconstruction with the implicit treatment of the damping term. We use different space steps  $\Delta x = \{5 \times 10^{-2}, 2.5 \times 10^{-2}, 10^{-2}, 5 \times 10^{-3}, 2.5 \times 10^{-3}\}$ .

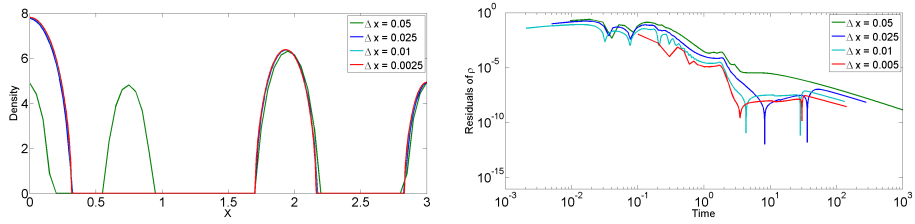


FIGURE 5. Mesh refinement in the case  $\gamma=3$ . Density distribution as a function of space (on the left) and residuals of the density as a function of time in a log-log scale (on the right) for the model (3) with  $\chi=10$ ,  $D=0.1$ ,  $a=20$ ,  $b=10$ ,  $\alpha=\kappa=1$  and  $\gamma=3$ , approximated using the P-reconstruction with the implicit treatment of the damping term. We use different space steps  $\Delta x = \{5 \times 10^{-2}, 2.5 \times 10^{-2}, 10^{-2}, 5 \times 10^{-3}\}$ .

solution for the mesh of size  $\Delta x = 5 \times 10^{-3}$  is the same for  $\gamma=2$  and  $\gamma=3$ , that is to say three bumps.

## 5. NUMERICAL COMPARISON OF THE ASYMPTOTIC BEHAVIOR OF THE SOLUTIONS TO THE QUASILINEAR HYPERBOLIC AND THE DEGENERATE PARABOLIC SYSTEMS

As explained before, on bounded domains with no-flux boundary conditions, stationary solutions for quasilinear hyperbolic system (3) and parabolic system (1) are the same. A complete description of such stationary solutions has been recalled in Section 2. Since we observed in [34] that some of these stationary solutions with several bumps are asymptotic states of system (3), we expect these solutions to be also asymptotic solutions of the parabolic model (1). This guess is motivated by the convergence of the solutions to the hyperbolic problem towards a parabolic-elliptic model in the

LTLTD limit; see [29] for the model (3) without chemotaxis on unbounded domain and [11] for the full model, still on an unbounded domain.

Therefore, in this section, our goal is to compare carefully the large time behavior of these two models. First, we analyze the asymptotic solutions for initial data given by stationary solutions, which are computed explicitly in the case  $\gamma=2$ . Notice that, due to numerical errors, the solutions are no longer stationary. In the case of a non-symmetric stationary solution composed of two lateral half bumps with different masses, we find that the asymptotic solutions of the two models are different. In the same way, for  $\gamma=3$ , we choose a generic initial datum and we give examples of parameters for which the two systems stabilize asymptotically on different solutions; also in that case, we show evidences of the appearance and disappearance of some metastable patterns.

Before the analysis of the asymptotic behavior of the solutions, we briefly present an accurate scheme for the parabolic model (1) based on a relaxation technique.

**5.1. Numerical discretization of degenerate parabolic model.** Now we describe the numerical scheme we use for the Keller-Segel type model (1). As in the case of the hyperbolic model, the linear reaction-diffusion equation for the chemical concentration  $\phi$  is solved using the second order centered finite differences method in space and a classical explicit-implicit Crank-Nicholson integration in time. At this point, we focus only on the equation for the time evolution of the density

$$\rho_t = (P(\rho)_x - \chi(\rho)\phi_x)_x, \quad (23)$$

where  $\chi(\rho) = \chi\rho$ .

Notice that, due to the presence of vacuum, the classical second order centered explicit scheme

$$\begin{aligned} \rho_i^{n+1} = \rho_i^n + \frac{\Delta t}{\Delta x^2} (P_{i+1}^n - 2P_i^n + P_{i-1}^n) \\ - \frac{\chi\Delta t}{2\Delta x^2} [(\rho_i^n + \rho_{i+1}^n)(\phi_{i+1}^n - \phi_i^n) - (\rho_{i-1}^n + \rho_i^n)(\phi_i^n - \phi_{i-1}^n)], \end{aligned}$$

where  $P_i^n = P(\rho_i^n)$ , fails to preserve the non negativity of the density [7]. This is the reason why we consider the relaxation technique, based on the diffusive BGK approximation, introduced in [1]. The advantage of this approach lies in a suitable modification of the diffusion term, split into the linear and nonlinear parts, which guarantees the stability.

Using the BGK approximation with two velocities  $\lambda_1 = -\lambda_2 = \lambda$ , we are reduced to discretize linear transport problems, which is done thanks to upwind method, see [1] for more details, and we obtain the following scheme in the finite volume framework

$$\rho_i^{n+1} = \rho_i^n + \frac{\Delta t}{\Delta x} \left( \mathcal{F}_{i+1/2}^n - \mathcal{F}_{i-1/2}^n \right),$$

with

$$\mathcal{F}_{i+1/2}^n = \mathcal{F}_{i+1/2}^{n,d1} + \mathcal{F}_{i+1/2}^{n,d2} + \mathcal{F}_{i+1/2}^{n,c}.$$

Here the numerical flux is decomposed in three distinct parts, a nonlinear diffusive part with pressure, a linear diffusive part on the density and an

advection part, taking into account the chemotactic term :

$$\begin{cases} \mathcal{F}_{i+1/2}^{n,d1} = \mathcal{F}^{\text{diff1}}(P_i^n, P_{i+1}^n) = \left( \frac{1}{\sqrt{2}\Delta x} - \frac{\lambda}{2\theta^2} \right) (P_{i+1}^n - P_i^n), \\ \mathcal{F}_{i+1/2}^{n,d2} = \mathcal{F}^{\text{diff2}}(\rho_i^n, \rho_{i+1}^n) = \frac{\lambda}{2} (\rho_{i+1}^n - \rho_i^n), \\ \mathcal{F}_{i+1/2}^{n,c} = \mathcal{F}^{\text{chem}}(A_i^n, A_{i+1}^n) = \frac{1}{2} (A_i^n + A_{i+1}^n), \end{cases}$$

where  $A_i^n = \chi \rho_i^n \frac{\phi_{i+1}^n - \phi_{i-1}^n}{2\Delta x}$  is a discretization of the term  $\chi \rho \phi_x$ . The following choice of the two remaining parameters  $\theta$  and  $\lambda$ ,

$$\theta = \max_{\rho} \sqrt{\frac{P'(\rho)}{1-\beta}}, \quad \lambda = \frac{\chi \max_{\phi} \phi_x}{\beta},$$

with  $\beta \in ]0, 1[$ , guarantees the monotonicity of the BGK approximation, while the stability is ensured by the following CFL condition (see again [1] for the details of the proofs):

$$\Delta t \leq \min \left\{ \frac{\Delta x}{\lambda}, \frac{\Delta x^2}{2\theta^2} \right\}.$$

In practice, we will take  $\beta = 0.95$ . The splitting of the diffusion term into a linear part and a nonlinear part gives the consistency for  $\Delta x, \Delta t \rightarrow 0$  and the presence of the artificial viscosity preserves the non negativity of the density at vacuum.

In the following sections, we compare the asymptotic behavior of the quasilinear hyperbolic model (3) and the asymptotic behavior of the parabolic Keller-Segel model (1) using the previously described numerical schemes.

**5.2. Case of two non-symmetric bumps as initial datum.** We consider the interval  $L=4$  and an initial datum composed of two lateral bumps with different masses. The solution is constructed using the formulas of Section 2.2 with  $L=1$  for each bump and  $M=1$  for the left bump and  $M=3$  for the right bump. The length of the support of each bump is the same since it is independent of the mass  $M$ . In Figure 6, we display the asymptotic solutions at time  $t=150$  for the hyperbolic and parabolic models (on the left) and the residuals of the density as a function of time in a log-log scale (on the right). For the hyperbolic model, the initial density is stable, while in the case of the parabolic model, the smallest bump merges with the largest bump around time  $t=10$ .

Remark that, in that case, we exhibit a set of parameters and initial data for which the two models, hyperbolic and parabolic, have different asymptotic behaviors. Namely, in that case, the diffusivity of the parabolic model does not permit to keep distinct bumps and leads to the emergence of a single bump structure.

**5.3. Generic initial data.** In the previous section, we observed a case of different asymptotic states for the hyperbolic and parabolic models, that is to say asymptotic solutions composed of a different number of bumps. Now, we compare the behavior of the two systems for a generic initial datum. More precisely, we consider an interval of length  $L=3$  with some

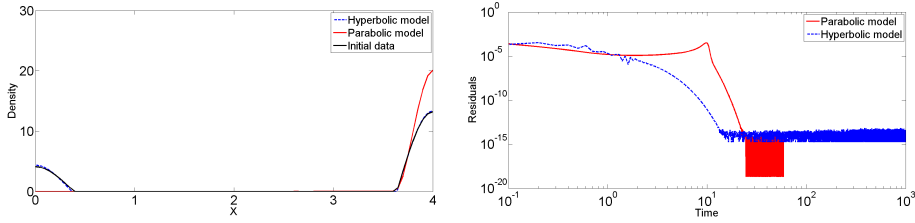


FIGURE 6. Density distributions as a function of space at the asymptotic states (on the left) and the residuals of the density as a function of time in the log-log scale (on the right) for the quasilinear hyperbolic model (3) and the parabolic Keller-Segel system (1) with  $\gamma=2$ ,  $\chi=50$ ,  $D=a=b=\alpha=\kappa=1$  and the exact, non-symmetric steady solution composed of two lateral bumps with different masses as initial datum.

parameters  $\chi=10$ ,  $D=0.1$ ,  $a=20$ ,  $b=10$ ,  $\kappa=\alpha=1$  and  $\gamma=3$ ; we take as an initial density the function  $\rho_0(x) = 1.5 + \sin(4\pi|x - 0.25L|)$  and the initial condition for the concentration  $\phi$  is  $\phi_0=0$ . In Section 4, we studied the dependence of the solutions of the hyperbolic model on the mesh refinement. We observed a high sensitivity to the space step in the case  $\gamma=2$ . That is why, to avoid possible inaccurate results, we consider now only the case  $\gamma=3$ , for which the acceptable grid size is much larger. In the following test, we perform simulations on a mesh with space step  $\Delta x=0.01$ . The solution of the hyperbolic system was also verified on a finer mesh with  $\Delta x=0.005$  and the density distribution did not change.

In Figure 7, we present the density at different times for the quasilinear hyperbolic model and the parabolic system. In the case of the parabolic model, we observe some metastable patterns. This phenomenon has been already observed, but without vacuum, for the Keller-Segel type model with linear diffusion and logistic chemosensitive function, see [23]. For the parabolic model, we start with a smooth perturbation of an initial constant solution, and a "comb" structure with several bumps appears and remains almost unchanged for a while, that is to say between  $t \sim 2$  and  $t \sim 10$ . Then, a fast transition takes place and one of the interior bumps moves towards the boundary. This structure seems again to be frozen up to  $t \sim 300$  when another transition occurs and only one bump remains. Analyzing the residuals of the density in Figure 8, we note that the time between the subsequent transitions becomes larger as the number of bumps decreases.

Moreover, the initial evolution of the hyperbolic model is much faster and the interactions between bumps and the merging of some of them end between time  $t=10$  and  $t=20$ . In the end, one bump and two half bumps remain and the solution stabilizes, which is confirmed by the residuals of the density. Again, the hyperbolic and the parabolic asymptotic behaviors are different.

**Acknowledgement.** The authors thank François Bouchut for some useful suggestions. This work has been partially supported by the project

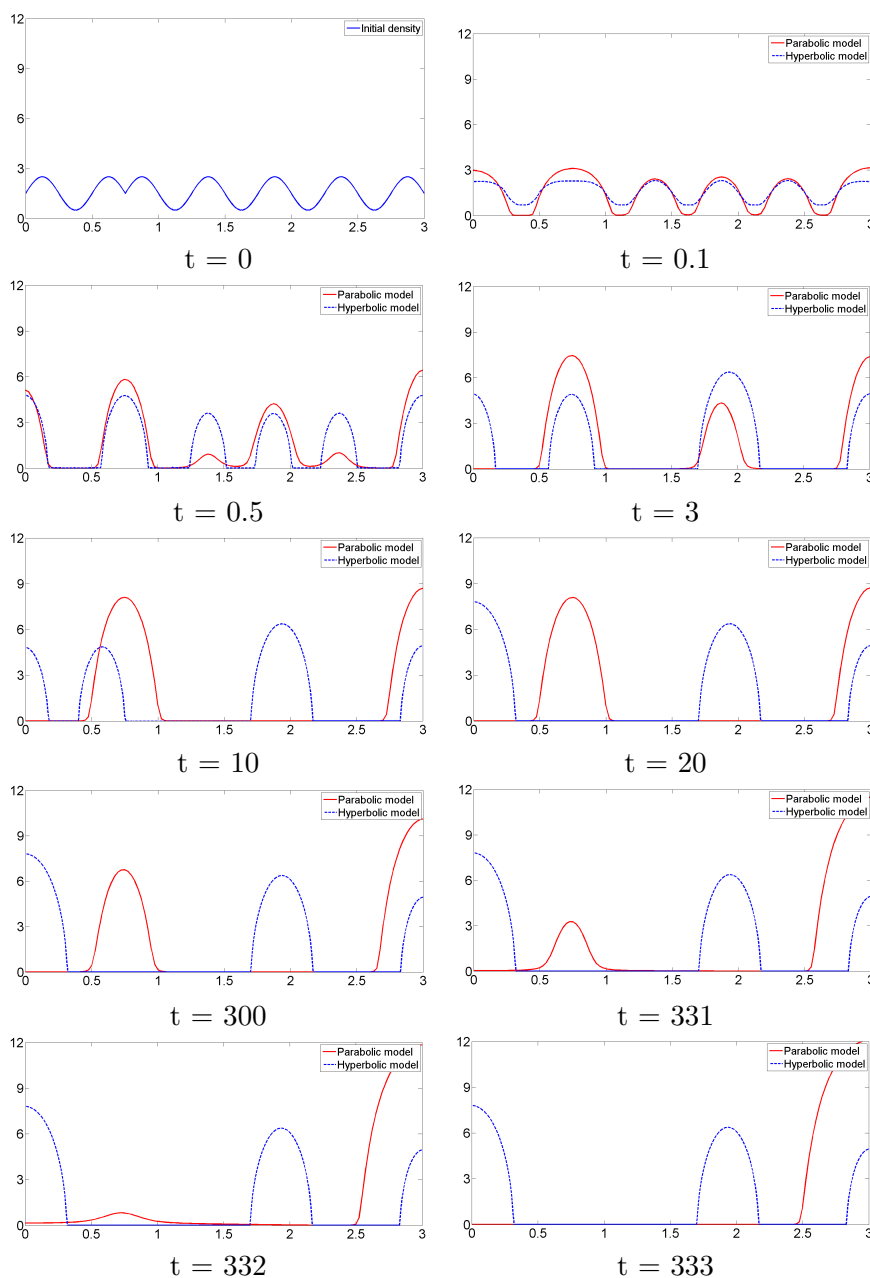


FIGURE 7. Density  $\rho$  as a function of space at different times for the quasilinear hyperbolic model of chemotaxis (3) and for the Keller-Segel system (1) with  $\chi = 10$ ,  $D = 0.1$ ,  $a = 20$ ,  $b = 10$ ,  $\kappa = \alpha = 1$  and  $\gamma = 3$ . The initial data are  $\rho_0(x) = 1.5 + \sin(4\pi|x - 0.25L|)$  and  $\phi_0(x) = 0$ .

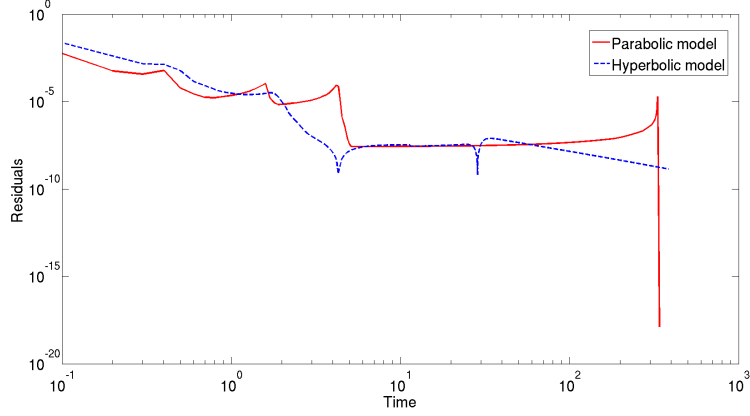


FIGURE 8. Residuals of the density as a function of time in a log-log scale for the quasilinear hyperbolic model of chemotaxis (3) and the Keller-Segel system (1) with  $\chi = 10$ ,  $D = 0.1$ ,  $a = 20$ ,  $b = 10$ ,  $\kappa = \alpha = 1$  and  $\gamma = 3$ . The initial data are  $\rho_0(x) = 1.5 + \sin(4\pi|x - 0.25L|)$  and  $\phi_0(x) = 0$ .

## 6. ANNEX : NUMERICAL FLUXES AND DEFINITION 3.1

Let us first recall the definition 3.1. A strongly consistent numerical flux  $\mathcal{F}$  satisfies the two following conditions :

$$\begin{cases} \text{if } \mathcal{F}^{\rho u}(r, 0, R, 0) = P(r), \text{ then } r = R; \\ \text{if } \mathcal{F}^{\rho u}(r, 0, R, 0) = P(R), \text{ then } r = R. \end{cases} \quad (24)$$

We consider the following equations :

$$\mathcal{F}^{\rho u}(r_{i+1/2}^{n,-}, 0, r_{i+1/2}^{n,+}, 0) - \mathcal{F}^{\rho u}(r_{i-1/2}^{n,-}, 0, r_{i-1/2}^{n,+}, 0) = P(r_{i+1/2}^{n,-}) - P(r_{i-1/2}^{n,+}), \quad (25)$$

computed at the beginning of the proof of Theorem 3.2. In the following, we will prove that conditions (24) are necessary and sufficient conditions to ensure that the equalities  $r_{i-1/2}^{n,-} = r_{i-1/2}^{n,+}$  for all  $i$  are the unique solutions of equations (25). We will also show that the following classical fluxes : HLL, HLL-Roe and Suliciu relaxation flux adapted to vacuum are indeed strongly consistent fluxes.

Remark that conditions (24) have already been derived as necessary conditions on the flux in [7], where a sufficient condition on the flux is also given to ensure the uniqueness property for the solutions of equations (25). Since we are dealing here with the bounded domain case with boundary conditions (4), our computations are slightly different from the ones of [7] and we are able to prove that the conditions (24) are also sufficient conditions.

Indeed, considering equations (25) for all  $i$ , using that  $r_{1/2}^{n,-} = r_{1/2}^{n,+}$  thanks to boundary conditions and using that the flux  $\mathcal{F}$  is consistent, a straightforward induction implies that

$$\mathcal{F}^{\rho u}(r_{i+1/2}^{n,-}, 0, r_{i+1/2}^{n,+}, 0) = P(r_{i+1/2}^{n,-}), \text{ for all } i. \quad (26)$$

Using condition (24), we obtain that  $r_{i-1/2}^{n,-} = r_{i-1/2}^{n,+}$  for all  $i$ . Therefore, condition (24) is a necessary and sufficient condition to guarantee that the equalities  $r_{i-1/2}^{n,-} = r_{i-1/2}^{n,+}$  for all  $i$  are unique solutions of equations (25).

Now, let us show that HLL, HLL-Roe and Suliciu with vacuum fluxes satisfy conditions (24). We assume in the following that the functions  $P$  and  $P'$  are increasing, as satisfied by the pressure (2) we consider here.

**HLL flux.** The definition of HLL flux is given at eq. (2.111) in Bouchut's book [6] and we can compute

$$\mathcal{F}^{\rho u}(r, 0, R, 0) = \frac{c_2 P(r) - c_1 P(R)}{c_2 - c_1},$$

with  $c_1 = \min(-\sqrt{P'(r)}, -\sqrt{P'(R)})$  and  $c_2 = \max(\sqrt{P'(r)}, \sqrt{P'(R)})$ , that is to say

$$\mathcal{F}^{\rho u}(r, 0, R, 0) = \frac{P(r) + P(R)}{2},$$

which satisfies clearly conditions (24).

**HLL-Roe flux.** In [16], we can find a version of the HLL flux adapted to vacuum. In that case,

$$\mathcal{F}^{\rho u}(r, 0, R, 0) = \frac{c_2 P(r) - c_1 P(R)}{c_2 - c_1},$$

with  $c_1 = \min(-\sqrt{P'(r)}, -\bar{c})$  and  $c_2 = \max(\bar{c}, \sqrt{P'(R)})$ , where  $\bar{c} = \sqrt{\frac{\sqrt{R}P'(R) + \sqrt{r}P'(r)}{\sqrt{R} + \sqrt{r}}}$ , that is to say

$$\mathcal{F}^{\rho u}(r, 0, R, 0) = \begin{cases} \frac{\sqrt{P'(R)}P(r) + \bar{c}P(R)}{\sqrt{P'(R)} + \bar{c}}, & \text{if } R > r, \\ \frac{\bar{c}P(r) + \sqrt{P'(r)}P(R)}{\bar{c} + \sqrt{P'(r)}}, & \text{if } r > R. \end{cases}$$

From this expression, we conclude easily that HLL-Roe flux satisfies conditions (24).

**Suliciu flux adapted to vacuum.** Now, we consider the Suliciu relaxation flux adapted to vacuum, which expression can be found in [6] at equations (2.133)-(2.136).

If  $0 < r < R$ , a standard computation leads to

$$\mathcal{F}^{\rho u}(r, 0, R, 0) = \frac{c_2 P(r) + c_1 P(R)}{c_1 + c_2} + \frac{Rc_2}{c_1 + c_2} \times \frac{(P(r) - P(R))^2}{c_2(c_1 + c_2) + R(P(R) - P(r))},$$

with  $c_1 = r\sqrt{P'(r)} + \alpha r \left( \frac{P(R) - P(r)}{R\sqrt{P'(R)}} \right) > 0$  and  $c_2 = R\sqrt{P'(R)} > 0$ .

If  $r > R > 0$ , we obtain a similar formula, namely

$$\mathcal{F}^{\rho u}(r, 0, R, 0) = \frac{c_2 P(r) + c_1 P(R)}{c_1 + c_2} + \frac{rc_1}{c_1 + c_2} \times \frac{(P(r) - P(R))^2}{c_1(c_1 + c_2) + r(P(r) - P(R))},$$

with  $c_1 = r\sqrt{P'(r)} > 0$  and  $c_2 = R\sqrt{P'(R)} + \alpha R \left( \frac{P(r) - P(R)}{r\sqrt{P'(r)}} \right) > 0$ .

Now, we consider the equation  $\mathcal{F}^{\rho u}(r, 0, R, 0) = P(r)$ . On the one hand, in the case  $r < R$ ,

$$\begin{aligned} 0 &= \mathcal{F}^{\rho u}(r, 0, R, 0) - P(r) \\ &= \frac{c_1(P(R) - P(r))}{c_1 + c_2} + \frac{Rc_2}{c_1 + c_2} \times \frac{(P(r) - P(R))^2}{c_2(c_1 + c_2) + R(P(R) - P(r))}. \end{aligned}$$

Since the right-hand side of the last equation is the sum of two positive terms, it is straightforward that they are both null and that  $P(R) = P(r)$ , which leads to  $R = r$ . On the other hand, in the case  $r > R$ ,

$$\begin{aligned} 0 &= \mathcal{F}^{\rho u}(r, 0, R, 0) - P(r) \\ &= \frac{c_1(P(R) - P(r))}{c_1 + c_2} + \frac{rc_1}{c_1 + c_2} \times \frac{(P(r) - P(R))^2}{c_1(c_1 + c_2) + r(P(r) - P(R))}. \end{aligned}$$

This equation can be simplified as :

$$c_1(c_1 + c_2) = 0 \text{ or } P(r) - P(R) = 0.$$

Since the first equality is impossible, we conclude that  $r = R$ .

Notice that the equation  $\mathcal{F}^{\rho u}(r, 0, R, 0) = P(R)$  can be treated in a similar way. Therefore, we have proved that the Suliciu relaxation flux satisfies also the conditions (24).

## REFERENCES

- [1] D. Aregba-Driollet, R. Natalini, and S. Tang. Explicit diffusive kinetic schemes for nonlinear degenerate parabolic systems. *Math. Comp.*, 73(245):63–94 (electronic), 2004.
- [2] E. Audusse, F. Bouchut, M. O. Bristeau, R. Klein, and B. Perthame. A fast and stable well-balanced scheme with hydrostatic reconstruction for shallow water flows. *SIAM Journal on Scientific Computing*, 25(6):2050, 2004.
- [3] F. Berthelin, D. Chiron, and M. Ribot. Classification of some stationary solutions with vacuum for a quasilinear system of chemotaxis. *in preparation*, 2014.
- [4] P. Biler, I. Guerra, and G. Karch. Large global-in-time solutions of the parabolic-parabolic keller-segel system on the plane. *ArXiv e-prints 1401.7650*, jan 2014.
- [5] R. Botchorishvili, B. Perthame, and A. Vasseur. Equilibrium schemes for scalar conservation laws with stiff sources. *Math. Comp.*, 72(241):131–157 (electronic), 2003.
- [6] F. Bouchut. Nonlinear stability of finite volume methods for hyperbolic conservation laws, and well-balanced schemes for sources. In *Nonlinear stability of finite volume methods for hyperbolic conservation laws, and well-balanced schemes for sources*, Frontiers in Mathematics. Birkhauser, 2004.
- [7] F. Bouchut, H. Ounaissa, and B. Perthame. Upwinding of the source term at interfaces for Euler equations with high friction. *Comput. Math. Appl.*, 53(3-4):361–375, 2007.
- [8] V. Calvez and J.A. Carrillo. Volume effects in the kellersegel model: energy estimates preventing blow-up. *J. Math. Pures Appl.*, 86:155175, 2006.
- [9] V. Calvez and L. Corrias. The parabolic-parabolic Keller-Segel model in  $\mathbb{R}^2$ . *Commun. Math. Sci.*, 6(2):417–447, 2008.
- [10] V. Calvez, L. Corrias, and M. A. Ebde. Blow-up, concentration phenomenon and global existence for the Keller-Segel model in high dimension. *Comm. Partial Differential Equations*, 37(4):561–584, 2012.
- [11] M. Di Francesco and Donatelli D. Singular convergence of nonlinear hyperbolic chemotaxis systems to keller-segel type models. *Discrete and Continuous Dynamical Systems (B)*, 13(1):79–100, 2010.
- [12] C. Di Russo. Analysis and numerical approximations of hydrodynamical models of biological movements. *Rend. Mat. Appl. (7)*, 32(3-4):117–367, 2012.



- [13] C. Di Russo and A. Sepe. Existence and asymptotic behavior of solutions to a quasi-linear hyperbolic-parabolic model of vasculogenesis. *SIAM J. Math. Anal.*, 45(2):748–776, 2013.
- [14] Y. Dolak and T. Hillen. Cattaneo models for chemosensitive movement: numerical solution and pattern formation. *J Math Biol*, 46(5):461–78, 2003.
- [15] Y. Dolak and C. Schmeiser. The keller-segel model with logistic sensitivity function and small diffusivity. *SIAM J. Appl. Math.*, 66, 2006.
- [16] B. Einfeldt, C.-D. Munz, P. L. Roe, and B. Sjögreen. On Godunov-type methods near low densities. *J. Comput. Phys.*, 92(2):273–295, 1991.
- [17] A. Gamba, D. Ambrosi, A. Coniglio, A. de Candia, S. Di Talia, E. Giraudo, G. Serini, L. Preziosi, and F. Bussolino. Percolation, morphogenesis, and burgers dynamics in blood vessels formation. *Phys Rev Lett*, 90(11):118101, 2003.
- [18] L. Gosse. Maxwellian decay for well-balanced approximations of a super-characteristic chemotaxis model. *SIAM J. Scient. Comput.*, 34:A520–A545, 2012.
- [19] L. Gosse. *Computing qualitatively correct approximations of balance laws*, volume 2 of *SIMAI Springer Series*. Springer, Milan, 2013.
- [20] L. Gosse. A well-balanced scheme for kinetic models of chemotaxis derived from one-dimensional local forward-backward problems. *Math. Biosci.*, 242(2):117–128, 2013.
- [21] X. Gu and Z. Lei. Well-posedness of 1-D compressible Euler-Poisson equations with physical vacuum. *J. Differential Equations*, 252(3):2160–2188, 2012.
- [22] F. R. Guarguaglini, C. Mascia, R. Natalini, and M. Ribot. Stability of constant states of qualitative behavior of solutions to a one dimensional hyperbolic model of chemotaxis. *Discrete Contin. Dyn. Syst. Ser. B*, 12(1):39–76, 2009.
- [23] T. Hillen and K. Painter. Global existence for a parabolic chemotaxis model with prevention of overcrowding. *Advances in Applied Mathematics*, 26(4):280 – 301, 2001.
- [24] T. Hillen and A. Stevens. Hyperbolic models for chemotaxis in 1-d. *Nonlinear Anal.: Real World Appl.*, 1(3):409–433, September 2000.
- [25] D. Horstmann. From 1970 until present: the Keller-Segel model in chemotaxis and its consequences. I. *Jahresber. Deutsch. Math.-Verein.*, 105(3):103–165, 2003.
- [26] J. Jang and N. Masmoudi. Well-posedness for compressible Euler equations with physical vacuum singularity. *Comm. Pure Appl. Math.*, 62(10):1327–1385, 2009.
- [27] E.F. Keller and L.A. Segel. Initiation of slime mold aggregation viewed as an instability. *J. Theor. Biol.*, 26:399–415, 1970.
- [28] R. Kowalczyk. Preventing blow-up in a chemotaxis model. *Journal of Mathematical Analysis and Applications*, 305(2):566 – 588, 2005.
- [29] P. Marcati and A. Milani. The one-dimensional Darcy’s law as the limit of a compressible Euler flow. *J. Differential Equations*, 84(1):129–147, 1990.
- [30] J. D. Murray. *Mathematical biology. I*, volume 17 of *Interdisciplinary Applied Mathematics*. Springer-Verlag, New York, third edition, 2002. An introduction.
- [31] J. D. Murray. *Mathematical biology. II*, volume 18 of *Interdisciplinary Applied Mathematics*. Springer-Verlag, New York, third edition, 2003. Spatial models and biomedical applications.
- [32] T. Nagai and T. Yamada. Large time behavior of bounded solutions to a parabolic system of chemotaxis in the whole space. *J. Math. Anal. Appl.*, 336(1):704–726, 2007.
- [33] R. Natalini and M. Ribot. An asymptotic high order mass-preserving scheme for a hyperbolic model of chemotaxis. *SIAM J. Num. Anal.*, 50(2):883–905, 2012.
- [34] R. Natalini, M. Ribot, and M. Twarogowska. A well-balanced numerical scheme for a one dimensional quasilinear hyperbolic model of chemotaxis. *Communication Mathematical Science*, 12:13–29, 2014.
- [35] K. Painter and T. Hillen. Volume-filling and quorum sensing in models for chemosensitive movement. *Canadian Appl. Math. Quart.*, 10(4):501 – 543, 2002.
- [36] C. Patlak. Random walk with persistence and external bias. *The bulletin of mathematical biophysics*, 15(3):311–338, 1953.
- [37] B. Perthame. Pde models for chemotactic movements: Parabolic, hyperbolic and kinetic. *Applications of Mathematics*, 49(6):539–564, 2004.
- [38] B. Perthame. *Transport equations in biology*. Frontiers in Mathematics. Birkhäuser Verlag, Basel, 2007.

- [39] B. Perthame and C. Simeoni. Convergence of the upwind interface source method for hyperbolic conservation laws. In *Hyperbolic problems: theory, numerics, applications*, pages 61–78. Springer, Berlin, 2003.
- [40] A.B. Potapov and T. Hillen. Metastability in chemotaxis models. *J. Dyn. Differ. Equations*, 17(2):293–330, 2005.
- [41] G. Serini, D. Ambrosi, E. Giraudo, A. Gamba, L. Preziosi, and F. Bussolino. Modeling the early stages of vascular network assembly. *The EMBO Journal*, 22(8):1771–1779, 2003.